THE JOURNAL OF PHYSICAL CHEMISTRY LETTERS
A JOURNAL OF THE AMERICAN CHEMICAL SOCIETY

pubs.acs.org/JPCL

Letter

Using Spectator Ligands to Enhance Nanocrystal-to-Molecule Electron Transfer

Emily K. Raulerson, Danielle M. Cadena, Mohammed A. Jabed, Christopher D. Wight, Inki Lee, Holden R. Wagner, James T. Brewster, II, Brent L. Iverson, Svetlana Kilina,* and Sean T. Roberts*

Cite This: J. Phys. Chem. Lett. 2022, 13, 1416−1423

Read Online

ACCESS | Metrics & More | Article Recommendations | Supporting Information

ABSTRACT: Semiconductor nanocrystals (NCs) have emerged as promising photocatalysts. However, NCs are often functionalized with complex ligand shells that contain not only charge acceptors but also other "spectator ligands" that control NC solubility and affinity for target reactants. Here, we show that spectator ligands are not passive observers of photoinduced charge transfer but rather play an active role in this process. We find the rate of electron transfer from quantum-confined PbS NCs to perylenediimide acceptors can be varied by over a factor of 4 simply by coordinating cinnamate ligands with distinct dipole moments to NC surfaces. Theoretical calculations indicate this rate variation stems from both ligand-induced changes in the free energy for charge transfer and electrostatic interactions that alter perylenediimide electron acceptor orientation on NC surfaces. Our work shows NC-to-molecule charge transfer can be fine-tuned through ligand shell design, giving researchers an additional handle for enhancing NC photocatalysis.

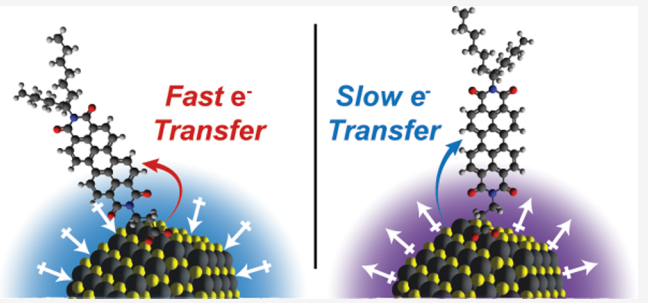

Because of their size-tunable electronic properties, quantum-confined nanocrystals (NCs) have emerged as a premier design platform for optoelectronics, sensors, and imaging agents.[1−9] More recently, the high molar absorptivity, large surface areas for substrate binding, and readily tunable redox properties of NCs have led to exploration of their use as photocatalysts.[10−15] However, to function effectively in this role, NCs must be able to exchange charge with molecules in their environment, which necessitates orbital overlap between a NC charge donor and molecular acceptor. An effective strategy for achieving such overlap has been to directly coordinate charge acceptors to NC surfaces via short chemical tethers.[16−23] Several studies have interrogated how the structure of these linkages controls the rate of photoinduced charge transfer, finding that this rate generally scales exponentially with the spatial separation between a NC and the charge acceptor.[16,21−24]

Less explored is how the NC ligand shell that surrounds a charge acceptor acts to mediate charge transfer. NCs are often decorated with ligand shells that impart several key properties to the NC, such as solubility in distinct chemical environments and the ability to bind specific target reactants. While only a few of the ligands bound to a NC may function as a charge acceptor, the other "spectator ligands" bound to the NC can play an important role in guiding charge transfer.

Figure 1 summarizes two mechanisms by which spectator ligands can alter rates for photoinduced charge transfer. In the first (left), spectator ligands containing static dipole moments produce an electric field that, depending on its alignment, will raise or lower the free energy for transferring a charge from a NC to a molecule bound to its surface. This approach of binding polar molecules to a surface has been used to tune the work function of planar semiconductors employed for solar energy and fuels generation[25−31] and was recently utilized by Beard and co-workers to vary the work function of PbS NCs over a 2 eV range.[32] However, while increasing ΔG° for photoinduced NC-to-molecule charge transfer can improve its rate, it will come at a cost as a smaller fraction of an absorbed photon's energy will be stored in the resulting products.

Specific steric or electrostatic interactions between charge acceptors and spectator ligands can also alter how charge acceptors orient themselves with respect to a NC surface (Figure 1, right).[33] As charge transfer exhibits an exponential dependence on the distance between the NC and acceptor, conformational fluctuations that modify this distance can play a major role in setting the rate of charge transfer. For example, introducing ligands that pack tightly on a surface can slow charge transfer by hindering a charge acceptor's ability to undergo transient structural fluctuations that move it closer to the NC surface.[34,35] In contrast, engineering attractive

Received: November 21, 2021
Accepted: January 31, 2022
Published: February 4, 2022

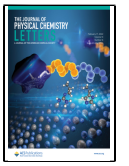

https://doi.org/10.1021/acs.jpclett.1c03825
J. Phys. Chem. Lett. 2022, 13, 1416−1423

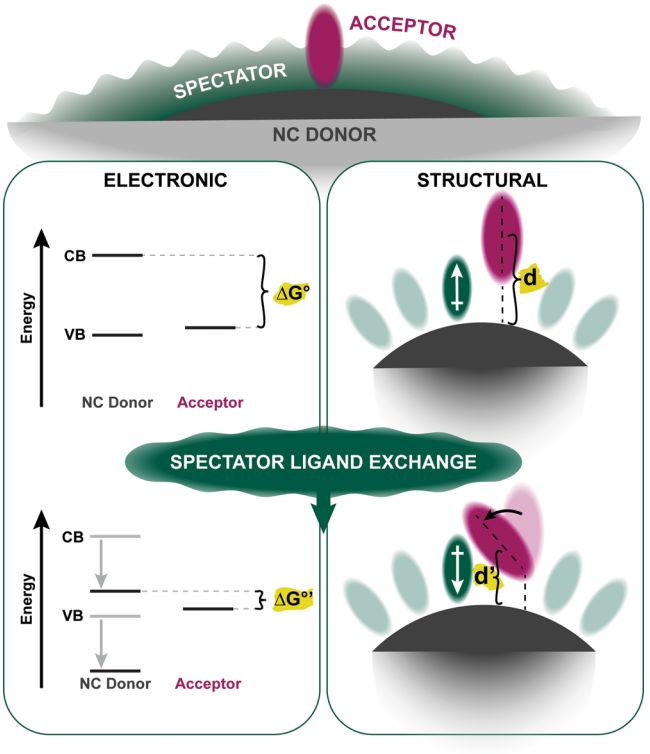

Figure 1. Spectator ligands can impact the rate of charge transfer from a NC donor to a molecular acceptor via two mechanisms: (left) electronic perturbation, wherein spectator ligands alter a NC's work function and thereby the free energy change for charge transfer ($\Delta G°$); (right) structural perturbation, wherein spectator ligands alter the distance between charge acceptors and the NC surface (d), thereby altering their electronic coupling.

electrostatic interactions between charge acceptors and short spectator ligands that draw acceptors toward the NC surface should speed charge transfer. The acceptor's orientation on the NC surface and resulting charge transfer dynamics can also be impacted by the chemical composition of the spectator ligand, which can alter solvation of the ligand shell[36] and thereby induce a change in the dielectric environment surrounding the charge acceptor.

In this report, we employ PbS NCs functionalized with perylenediimide (PDI) electron acceptors to assess the ability of spectator ligands to impact photoinduced electron transfer rates. As spectator ligands, we employ a family of cinnamate molecules whose static dipole moments can be readily altered by introducing fluorine atoms at different positions along their periphery. We find these structural modifications alter the rate of PbS-to-PDI electron transfer by upward of a factor of 4. Using electronic structure calculations based on density functional theory (DFT), we separate energetic and structural contributions to this rate variation. We find that while the dipole moments of cinnamate ligands shift $\Delta G°$ for electron transfer by 50 meV, this alone is insufficient to fully explain the rate variation we observe. Rather, we find a key contribution to the rate variation stems from directional electrostatic interactions between cinnamate ligands and PDI electron acceptors that tune the effective distance over which electron transfer occurs. Our work shows that, rather than functioning as passive observers, spectator ligands are an active participant in NC-to-molecule charge transfer. This affords new opportunities for controlling NC-driven charge transfer by shaping the ligand environment in which it takes place.

A two-step ligand exchange process was used to install a spectator ligand shell and PDI acceptor molecules on the surface of PbS NCs natively functionalized with oleate (Scheme 1, OA^-). PDIs were chosen as an appropriate

Scheme 1. Chemical Structures of Spectator Ligands and PDI Electron Acceptor

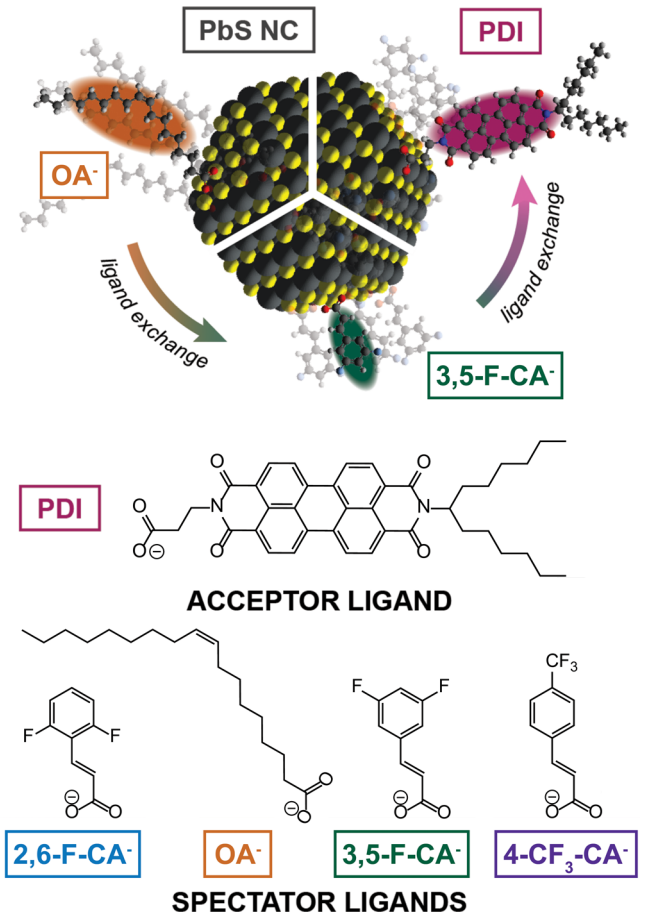

electron acceptor to pair with PbS as their LUMO energy (−3.9 eV with respect to vacuum)[37,38] falls below the conduction band edge (−3.6 eV)[39] of the 3.1 nm diameter PbS NCs we employ. We functionalized one of the PDIs' imide positions with a short two-carbon chain terminated with a carboxylate group to allow attachment to PbS. A swallowtail carbon chain was affixed to the other PDI imide position to promote solubility in organic solvents (see the Supporting Information for synthetic details). We chose a series of cinnamate derivatives to employ as spectator ligands to study how the chemical composition of a PbS NC's ligand shell impacts its ability to donate charge. These ligands can undergo quantitative exchange with OA^- ligands native to the NC synthesis while continuing to impart colloidal solubility.[40] Importantly, Kroupa et al. reported that dipoles introduced by cinnamate ligands at the surface of a PbS NC can tune the band edge of a NC thin film over an ∼2 eV range with respect to vacuum.[32] Such shifts, if maintained for short-range electron transfer between NCs and surface-bound electron acceptors, will strongly alter the rate of this process according to Marcus theory.[41,42]

https://doi.org/10.1021/acs.jpclett.1c03825
J. Phys. Chem. Lett. 2022, 13, 1416−1423

After exchanging native OA^- ligands for a given cinnamate derivative, PDI molecules were added to NC surfaces. To eliminate unbound PDI monomers in solution, ligand-exchanged solutions were centrifuged, and the resulting pellet was resuspended. Absorption spectra of PbS NCs are shown following cinnamate ligand exchange and subsequent functionalization with PDI in Figure S3. We observe no major change in the PbS first exciton peak upon exchanging OA^- for cinnamate ligands or following subsequent functionalization with PDI. Subtraction of PbS contributions to absorption spectra allows for quantification of the average number of bound PDI molecules per NC, N_{PDI}, by comparing these features to extinction spectra of PDI monomers. This analysis indicates that the average number of bound PDIs per NC is 10−25 depending on the sample. At these concentrations, PDI absorption spectra show a redistribution of their vibrational progression that are suggestive of aggregate formation between surface-bound PDI molecules. Control measurements of NCs with low PDI surface concentrations wherein aggregation is absent (Figure S6) show the trends in PbS NC photoexcited dynamics highlighted below stem not from PDI aggregation but rather from changes in the composition of NC spectator ligand shells.

Following preparation of PbS NCs with mixed spectator/PDI ligand shells, we employed transient absorption spectroscopy (TA) to characterize their photoexcited dynamics. Figure 2A shows TA spectra of PbS:3,5-F-CA^-/PDI recorded following photoexcitation at 800 nm, which selectively excites PbS. At short time delays (red), a broad induced absorption across the visible spectral range is observed that has previously been assigned to PbS interband transitions.[43−46] As time progresses, these features decay into a sharper molecular signature with a ground-state bleach that peaks near 490 nm and a new induced absorption centered near 710 nm (blue). We assign this latter feature to the PDI radical anion as it matches previously reported experimental[47−49] and calculated[50] spectra of this species.

We have employed global target analysis to fit TA spectra recorded over the ∼2 ns time window of our experiment to the two-state rate model schematically depicted in Figure 2B. As charge transfer from PbS to PDI is expected to be exoergic by ∼300 meV (Supporting Information, section SVII), we can safely assume that back charge transfer, from PDI to PbS, will be negligible over the 2 ns time window of our experiment. Indeed, we find this model well reproduces the TA spectra (Figure S4), which allows us to extract from it a pair of species-associated spectra (SAS, Figure 2B) that we assign to interband transitions of the photoexcited PbS exciton and a $PbS^{\bullet+}$:$PDI^{\bullet-}$ charge-transfer state.

Figure 3 shows TA kinetic traces of PDI-functionalized PbS NCs whose ligand shells are composed of different spectator ligands. To highlight the growth of the $PbS^{\bullet+}$:$PDI^{\bullet-}$ charge transfer state, contributions to each spectrum from interband transitions of the PbS exciton have been removed via a background subtraction procedure (Supporting Information, section SVI). Spectra of each sample signal formation of a PDI radical anion as indicated by growth over time of an induced absorption near 710 nm and a photobleach of the PDI ground state near 490 nm. Application of our global target analysis model allows us to recover an electron transfer rate for each data set (k_{ET}, Table 1). These rates constitute an average of the electron transfer kinetics that occur for each individual NC within a sample, which are expected to vary across a NC ensemble as each NC can bind different numbers of PDI electron acceptors. Under the assumption that each NC's electron transfer rate increases linearly with the number of acceptors it binds, these ensemble-averaged transfer rates can be reanalyzed assuming that PDI acceptors are distributed among NCs according to a Poisson distribution (Supporting Information, section SV). This allows us to determine the intrinsic time scale for electron transfer between a PbS NC and a single PDI molecule bound to its surface, $k_{ET,int}$.

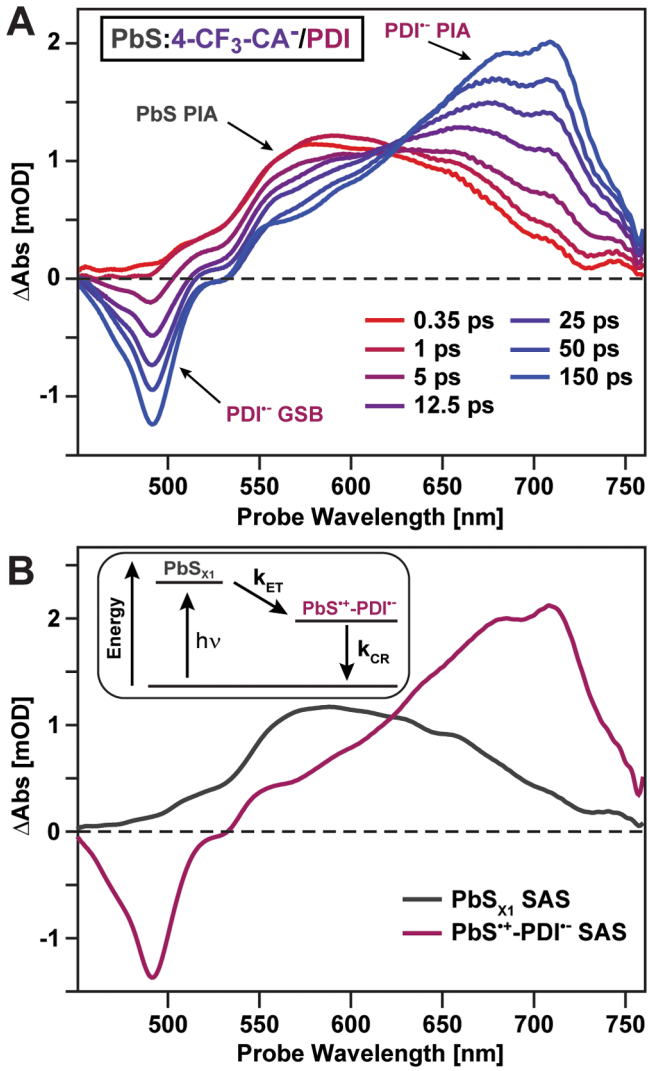

Figure 2. (A) TA spectra of PbS:4-CF_3-CA^-/PDI following photoexcitation at 800 nm. PIA: photoinduced absorption. GSB: ground-state bleach. (B) Species-associated spectra (SAS) extracted from data in (A) via application of the kinetic model shown in the inset. k_{ET} corresponds to the PbS-to-PDI electron transfer rate while k_{CR} is the relaxation rate of the PDI radical anion.

Comparing values of $k_{ET,int}$, we find electron transfer occurs fastest for PbS NCs functionalized with 2,6-F-CA^- and slows, in order, as the spectator shell is replaced by OA^-, 3,5-F-CA^-, and 4-CF_3-CA^-. This trend tracks with the strength of the spectator ligands' static dipole moment, which switches in sign from positive to negative moving from 2,6-F-CA^- to 4-CF_3−CA^-.[32] As the ligand dipole moment decreases, it will become increasingly more difficult to remove a negative charge from PbS and transfer it to a vacuum, resulting in a lowering (i.e., stabilization) of the PbS conduction band edge. If the energy

https://doi.org/10.1021/acs.jpclett.1c03825
J. Phys. Chem. Lett. 2022, 13, 1416−1423

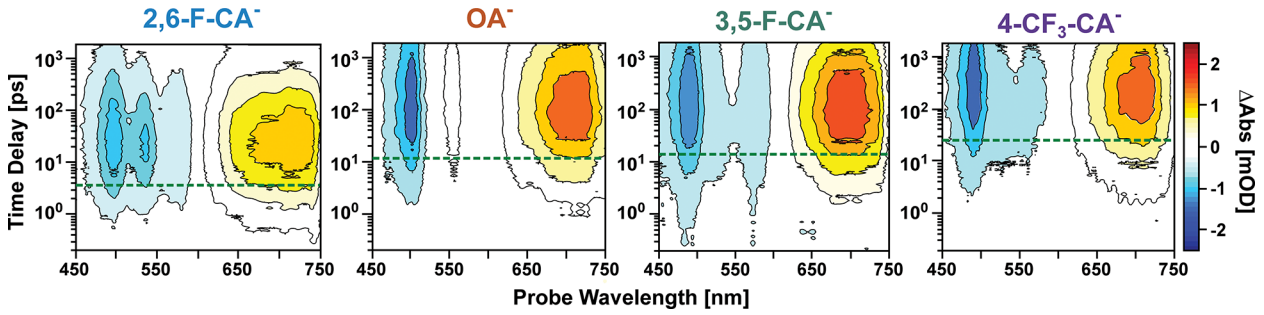

Figure 3. TA contours highlighting formation of the $PbS^{\bullet+}$:$PDI^{\bullet-}$ charge transfer state for PbS NCs functionalized with different spectator ligands. Spectral contributions from PbS interband transitions have been removed by using a background subtraction procedure. Dashed green lines represent values of k_{ET} extracted from global target analysis.

Table 1. Observed PbS-to-PDI Electron Transfer Rates (k_{ET}) and Intrinsic Electron Transfer Rates ($k_{ET,int}$) That Account for Differences in the Average Number of PDI Molecules Bound to PbS NCs in Each Sample (N_{PDI})[a]

	2,6-F-CA⁻	OA⁻	3,5-F-CA⁻	4-CF_3-CA⁻
$\langle N_{PDI} \rangle$	18.8 ± 1.6	10.7 ± 0.9	15.6 ± 1.3	11.3 ± 1.0
$1/k_{ET}$ [ps]	3.75	11.6	13.9	23.8
$1/k_{ET,int}$ [ps]	60 ± 3	107 ± 10	199 ± 5	242 ± 25

[a] $k_{ET,int}$ is calculated assuming bound PDI molecules are distributed among PbS NCs according to Poisson statistics.

of the PDI LUMO is unaffected by the spectator ligand dipole moment, lowering the PbS conduction band edge will decrease $\Delta G°$ for charge transfer. According to a Marcus theory model that accounts for electron−hole interactions in quantum-confined NCs,[42] this decrease in driving force should lower $k_{ET,int}$.

While this energetic argument based on the dipole moments of the spectator ligands is qualitatively consistent with the trend in $k_{ET,int}$ we observe, we find the magnitude of $k_{ET,int}$'s variation as we move across our spectator series is smaller than we would have anticipated based on prior photoelectron spectroscopy measurements of cinnamate-functionalized PbS NCs.[32] This work reported that the cinnamate ligands we have investigated can shift PbS's conduction band edge over a 2 eV range, which should alter $\Delta G°$ for charge transfer from being exergonic for 2,6-F-CA^- to strongly endergonic for 4-CF_3-CA^-. Such a driving force variation should fully suppress charge transfer from both 3,5-F-CA^- and 4-CF_3-CA^- functionalized NCs to PDI ligands, which disagrees with our experimental observations. This discrepancy may be due to several effects, such as screening of the spectator ligand dipoles by the solvent, a shifting of the PDI LUMO energy induced by interaction with the spectator ligands, or the close proximity of PDI electron acceptors to the PbS NC surface, which can nullify the impact of the electric field of the spectator ligand shell on electron transfer as electrons may not need to cross the full length of this field to move from PbS to PDI.

To untangle these effects, we have used DFT to examine the electronic structure of PbS NCs with different ligand shells. Figure 4 highlights the electronic structure computed for 1.5 nm $Pb_{44}S_{40}$ NCs featuring ligand shells composed of a single PDI molecule and seven spectator ligands (Supporting Information, section SVIII). As expected, we find the PbS conduction band edge moves relative to a vacuum as the composition of the ligand shell is varied. However, the range of its variation averaged over several different ligand shell

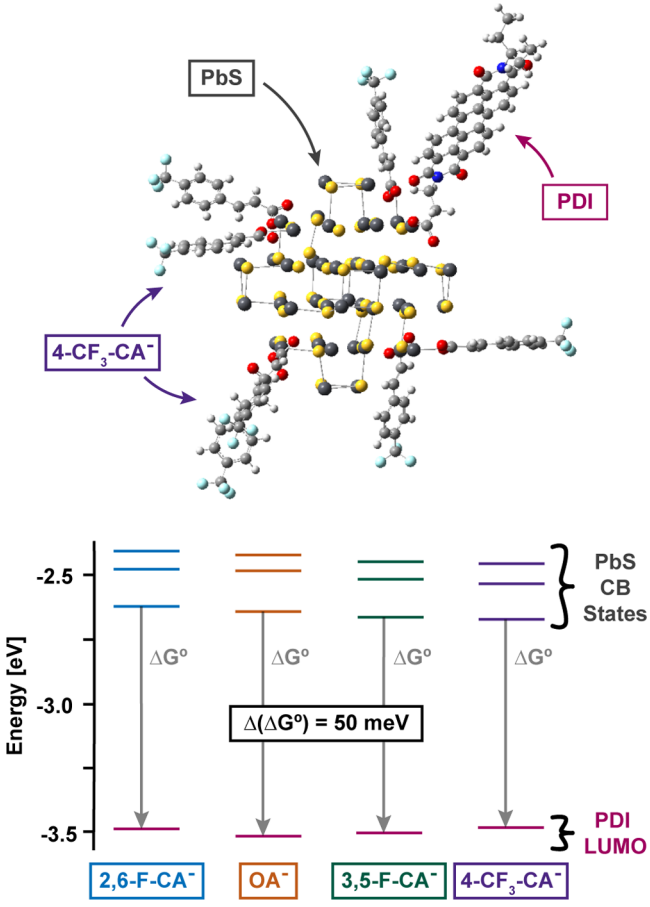

Figure 4. (top) Representative energy-minimized structure computed for PbS:4-CF_3-CA^-/PDI. (bottom) Computed energies for states that correspond to the PDI LUMO and PbS conduction band edge for PDI-functionalized PbS NCs with different spectator ligands. For all calculations, NCs were embedded in a polar medium whose dielectric properties match those of dichloromethane.

geometries is found to be only 60 meV when moving across the spectator ligand series. This indicates that solvent screening likely undermines the ability of spectator ligand dipoles to shift the conduction band edge. Indeed, we find that when the energy levels of our PbS NC model are recalculated in a vacuum as opposed to a polar medium meant to approximate dichloromethane, the range of variation of the PbS conduction band edge is increased by nearly a factor of 6.

Turning our focus to the free energy for electron transfer, $\Delta G°$, which we approximate as the energy difference between

https://doi.org/10.1021/acs.jpclett.1c03825
J. Phys. Chem. Lett. 2022, 13, 1416−1423

the PbS conduction band edge and PDI LUMO, we find this value varies by only 50 ± 100 meV moving across the spectator ligand series (Table S4). This result suggests that, within error, $\Delta G°$ may have zero dependence on spectator ligand identity. Moreover, assuming reasonable values of the reorganization energy for PbS-to-PDI electron transfer based on prior reports of NC-to-molecule electron transfer (200−500 meV),[42,51−54] we estimate changing $\Delta G°$ by 50 meV should at most lead to a 1.8× increase in $k_{ET,int}$ moving from 4-CF_3-CA^- to 2,6-F-CA^-. This is smaller than the (4.5 ± 0.4)× rate variation we observe experimentally. We note $k_{ET,int}$'s dependence on spectator ligand identity is enhanced even further as N_{PDI} is decreased (Figure S6). These observations suggest another effect apart from changes in $\Delta G°$ likely contributes to $k_{ET,int}$'s dependence on spectator ligand identity.

Examining the optimized structures derived from DFT, the experimentally measured PbS-to-PDI electron transfer rate shows a high degree of correlation with the molecular orientation of PDI on the PbS NC surface (Figure 5). As the dipole moments of the spectator ligands in our computed structures move from negative to positive values, PDI molecules are found to increasingly tilt toward the PbS surface. This bending results from the flexibility of the two-carbon chain linking PDIs to PbS, which allows PDIs to adjust their orientation in response to specific electrostatic interactions with neighboring spectator ligands. For example, 2,6-F-CA^- has an electron-deficient region at its most outward facing point (Figure S8) that can encourage neighboring, electron-rich PDIs to bend toward these ligands, decreasing their distance to the PbS surface (Figure 5A, left). In contrast, 4-CF_3-CA^- contains significant electron density at its most outward facing point. Surrounding a PDI by several 4-CF_3-CA^- ligands will therefore induce repulsive interactions that will, on net, favor orienting the PDI normal to the PbS surface (Figure 5A, right). We note tilting of PDI molecules induced by electrostatic interactions occurs in several structures optimized from distinct starting geometries, indicating this result is robust.

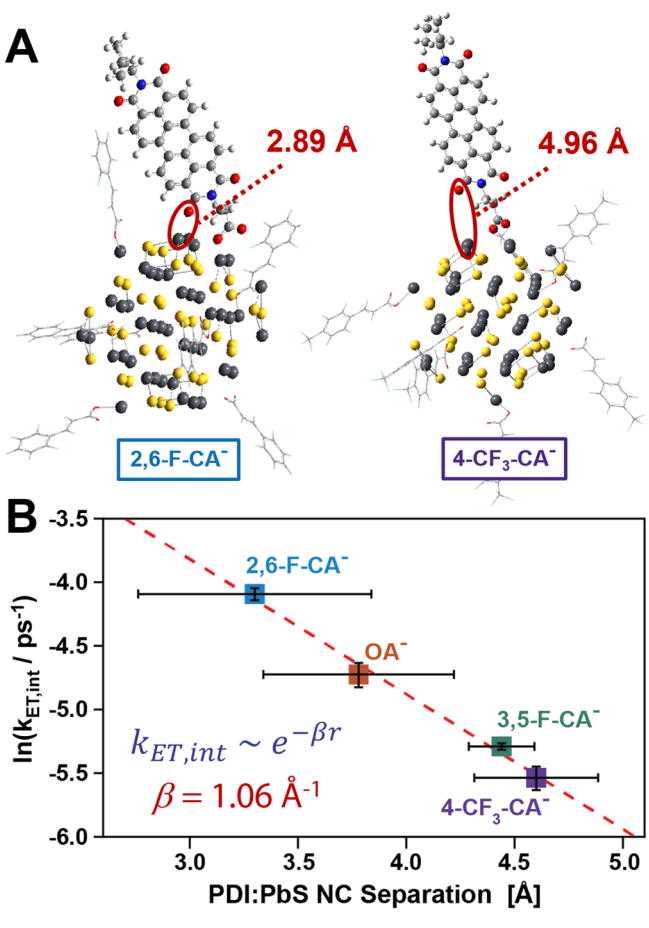

Figure 5. (A) Representative energy-minimized structures for PbS:PDI NCs featuring 2,6-F-CA^- and 4-CF_3-CA^- spectator ligands. Electrostatic interactions between 2,6-F-CA^- ligands and surface-anchored PDIs lead to a decrease in the distance between the PDI and PbS NC surface. (B) Comparison of experimentally measured values of $k_{ET,int}$ for PbS:PDI NCs featuring different spectator ligands and the average PDI:PbS spatial separation computed for each system. Error bars for the PDI:PbS NC separation represent the standard deviation of this value obtained from three distinct energy-minimized structures for each ligand set.

The DFT structures we have examined contain low loadings of spectator ligands due to computational cost. While this may raise a concern that these structures do not fully capture steric effects between ligands that are present on NCs with higher ligand densities, work by Weiss and co-workers has shown methylviologen electron acceptors bound to oleate-capped CdS NCs can tilt toward the NC surface even in the presence of high spectator ligand loading.[55] Such tilting could be reflective of preferential binding of electron acceptors to NC corner and edge sites that afford the electron acceptors higher orientation freedom. This hypothesis is supported by recent work by Green et al.,[56] who observed the preferential binding of 9-anthracenecarboxylic acid ligands to PbS NC corners and edges during ligand exchange. Thus, we believe that steric constraints placed on PDI electron acceptors due to surrounding spectator ligands are unlikely to fully suppress the ability of PDI ligands to tilt toward the surface of a PbS NC to which they are bound.

Our calculations suggest $k_{ET,int}$'s variation largely stems from changes in the orientation of PDI molecules on PbS surfaces that are dictated by electrostatic interactions between spectator ligands and PDI electron acceptors. The electronic coupling between PbS and PDI that allows for electron transfer depends on the spatial overlap of the PDI LUMO and states within the PbS conduction band. As this coupling decays exponentially with the distance between a PbS NC and PDI molecule, tilting PDIs toward a NCs' surface will enhance $k_{ET,int}$.

We can assess if changes in PbS:PDI spatial separation induced by spectator ligands is responsible for the observed variation in $k_{ET,int}$ by using the computed distance between the PbS surface and nearest PDI carbonyl oxygen to estimate the electron transfer distance. The optimized geometries for two of the spectator ligands, 4-CF_3-CA^- and 2,6-F-CA^-, are shown in Figure 5A. PDI core tilting is apparent in the case of the latter and leads to nearly a 2-fold difference in the spatial separation of the PbS electron donor and PDI acceptor between these structures. This separation is compared with $k_{ET,int}$ in Figure 5B, which reveals this rate indeed depends exponentially on the electron donor−acceptor distance. The β coefficient that describes the decrease of $k_{ET,int}$ with increasing donor−acceptor separation is 1.06 $Å^{-1}$, which is consistent with values reported for other NC-to-ligand electron transfer systems wherein the separation between the electron donor and acceptor is tuned by varying ligand length.[23,34] The strong dependence of $k_{ET,int}$ on PbS:PDI spatial separation highlights

https://doi.org/10.1021/acs.jpclett.1c03825
J. Phys. Chem. Lett. 2022, 13, 1416−1423

that the electronic coupling between these materials is weak. Ultrafast electron transfer is largely the result of the close spatial proximity of PbS and PDI, which our results indicate can be tuned by altering a NC's spectator ligand shell.

Additional evidence showing enhanced orbital overlap induced by the tilting of PDI molecules toward the PbS surface is provided by calculated optical absorption spectra of PDI-functionalized PbS NCs (Figure S10). We find that optical spectra of PbS:4-CF_3-CA^-/PDI consist of a sum of spectra computed from its individual PbS, PDI, and spectator ligand components, indicating electronic coupling between these components is weak. In contrast, spectra computed for PbS:2,6-F-CA^-/PDI are nonadditive as they show a noticeable deviation from the sum of spectra of the system's individual components. This suggests electronic coupling between PbS and PDI has been enhanced by replacing 4-CF_3-CA^- with 2,6-F-CA^-.

Our results show mixed-ligand surfaces can modulate charge transfer between PbS NCs and surface-bound electron acceptors by altering the average orientation adopted by the acceptors. Our observations demonstrate that spectator ligands are not benign, but rather play an active role in shaping interactions between NCs and electronically active molecules bound to their surface. This provides researchers with a new means for optimizing charge transfer between a NC and its environment. Using spectator ligands to alter the properties of NC interfaces is an approach orthogonal to varying NC quantum confinement and the redox properties of the charge acceptor. Altering these parameters, in concert with spectator ligand shell composition, can yield functional interfaces that robustly shuttle charge in a desired direction with minimal energetic loss.

■ ASSOCIATED CONTENT

Supporting Information

The Supporting Information is available free of charge at https://pubs.acs.org/doi/10.1021/acs.jpclett.1c03825.

> Synthetic methods used to prepare of PbS NCs with mixed cinnamate/PDI ligand shells; calculation of N_{PDI} from steady-state absorption spectra of functionalized PbS NCs; global target analysis applied to TA spectra to extract k_{ET}; determination of $k_{ET,int}$; discussion of the impact of PDI aggregation on $k_{ET,int}$; discussion of how changes in ΔG° impact $k_{ET,int}$ based on an Auger-assisted Marcus model; computational methods employed to examine the chemical and electronic structure of functionalized PbS NCs (PDF)

■ AUTHOR INFORMATION

Corresponding Authors

Svetlana Kilina − *Department of Chemistry and Biochemistry, North Dakota State University, Fargo, North Dakota 58108, United States;* orcid.org/0000-0003-1350-2790; Email: svetlana.kilina@ndsu.edu

Sean T. Roberts − *Department of Chemistry and Center for Dynamics and Control of Materials, The University of Texas at Austin, Austin, Texas 78712, United States;* orcid.org/0000-0002-3322-3687; Email: roberts@cm.utexas.edu

Authors

Emily K. Raulerson − *Department of Chemistry, The University of Texas at Austin, Austin, Texas 78712, United States*

Danielle M. Cadena − *Department of Chemistry, The University of Texas at Austin, Austin, Texas 78712, United States*

Mohammed A. Jabed − *Department of Chemistry and Biochemistry, North Dakota State University, Fargo, North Dakota 58108, United States;* orcid.org/0000-0001-8552-0301

Christopher D. Wight − *Department of Chemistry, The University of Texas at Austin, Austin, Texas 78712, United States;* orcid.org/0000-0003-3389-1762

Inki Lee − *Department of Chemistry, The University of Texas at Austin, Austin, Texas 78712, United States*

Holden R. Wagner − *Department of Chemistry, The University of Texas at Austin, Austin, Texas 78712, United States*

James T. Brewster, II − *Department of Chemistry, The University of Texas at Austin, Austin, Texas 78712, United States;* orcid.org/0000-0002-4579-8074

Brent L. Iverson − *Department of Chemistry, The University of Texas at Austin, Austin, Texas 78712, United States;* orcid.org/0000-0001-7974-3605

Complete contact information is available at: https://pubs.acs.org/10.1021/acs.jpclett.1c03825

Author Contributions

E.K.R. and D.M.C. contributed equally to this work.

Notes

The authors declare no competing financial interest.

■ ACKNOWLEDGMENTS

Work conducted at UT Austin was supported by the National Science Foundation (CHE-2003735), the Welch Foundation (F-1885 and F-1188), and Research Corporation for Science Advancement (24489). D.M.C. acknowledges support from the National Science Foundation Graduate Research Fellowship Program under Grant DGE-1610403. I.L. thanks UT Austin's Office of the Vice President of Research for support from an Undergraduate Research Fellowship. The computational work is supported by the National Science Foundation under Grant 2004197. For computational resources and administrative support, the authors acknowledge the Center for Computationally Assisted Science and Technology (CCAST) at North Dakota State University and the National Energy Research Scientific Computing Center (NERSC) supported by the Office of Science of the Department of Energy under Contract DE-AC02-05CH11231.

■ REFERENCES

(1) Talapin, D. V.; Lee, J.-S.; Kovalenko, M. V.; Shevchenko, E. V. Prospects of Colloidal Nanocrystals for Electronic and Optoelectronic Applications. *Chem. Rev.* **2010**, *110* (1), 389−458.

(2) Kagan, C. R.; Lifshitz, E.; Sargent, E. H.; Talapin, D. V. Building Devices from Colloidal Quantum Dots. *Science* **2016**, *353* (6302), aac5523.

(3) Kovalenko, M. V.; Manna, L.; Cabot, A.; Hens, Z.; Talapin, D. V.; Kagan, C. R.; Klimov, V. I.; Rogach, A. L.; Reiss, P.; Milliron, D. J.; Guyot-Sionnnest, P.; Konstantatos, G.; Parak, W. J.; Hyeon, T.; Korgel, B. A.; Murray, C. B.; Heiss, W. Prospects of Nanoscience with Nanocrystals. *ACS Nano* **2015**, *9* (2), 1012−1057.

(4) Shirasaki, Y.; Supran, G. J.; Bawendi, M. G.; Bulović, V. Emergence of Colloidal Quantum-Dot Light-Emitting Technologies. *Nat. Photonics* **2013**, *7* (1), 13−23.
(5) Chistyakov, A. A.; Zvaigzne, M. A.; Nikitenko, V. R.; Tameev, A. R.; Martynov, I. L.; Prezhdo, O. V. Optoelectronic Properties of Semiconductor Quantum Dot Solids for Photovoltaic Applications. *J. Phys. Chem. Lett.* **2017**, *8* (17), 4129−4139.
(6) Lu, H.; Huang, Z.; Martinez, M. S.; Johnson, J. C.; Luther, J. M.; Beard, M. C. Transforming Energy Using Quantum Dots. *Energy Environ. Sci.* **2020**, *13* (5), 1347−1376.
(7) Pietryga, J. M.; Park, Y.-S.; Lim, J.; Fidler, A. F.; Bae, W. K.; Brovelli, S.; Klimov, V. I. Spectroscopic and Device Aspects of Nanocrystal Quantum Dots. *Chem. Rev.* **2016**, *116* (18), 10513−10622.
(8) Tang, X.; Ackerman, M. M.; Chen, M.; Guyot-Sionnest, P. Dual-Band Infrared Imaging Using Stacked Colloidal Quantum Dot Photodiodes. *Nat. Photonics* **2019**, *13* (4), 277−282.
(9) García de Arquer, F. P.; Talapin, D. V.; Klimov, V. I.; Arakawa, Y.; Bayer, M.; Sargent, E. H. Semiconductor Quantum Dots: Technological Progress and Future Challenges. *Science* **2021**, *373* (6555), No. eaaz8541.
(10) Jensen, S. C.; Bettis Homan, S.; Weiss, E. A. Photocatalytic Conversion of Nitrobenzene to Aniline through Sequential Proton-Coupled One-Electron Transfers from a Cadmium Sulfide Quantum Dot. *J. Am. Chem. Soc.* **2016**, *138* (5), 1591−1600.
(11) Jiang, Y.; Wang, C.; Rogers, C. R.; Kodaimati, M. S.; Weiss, E. A. Regio- and Diastereoselective Intermolecular [2 + 2] Cycloadditions Photocatalysed by Quantum Dots. *Nat. Chem.* **2019**, *11* (11), 1034−1040.
(12) Caputo, J. A.; Frenette, L. C.; Zhao, N.; Sowers, K. L.; Krauss, T. D.; Weix, D. J. General and Efficient C−C Bond Forming Photoredox Catalysis with Semiconductor Quantum Dots. *J. Am. Chem. Soc.* **2017**, *139* (12), 4250−4253.
(13) Han, Z.; Qiu, F.; Eisenberg, R.; Holland, P. L.; Krauss, T. D. Robust Photogeneration of H_2 in Water Using Semiconductor Nanocrystals and a Nickel Catalyst. *Science* **2012**, *338* (6112), 1321.
(14) Huang, J.; Mulfort, K. L.; Du, P.; Chen, L. X. Photodriven Charge Separation Dynamics in CdSe/ZnS Core/Shell Quantum Dot/Cobaloxime Hybrid for Efficient Hydrogen Production. *J. Am. Chem. Soc.* **2012**, *134* (40), 16472−16475.
(15) Utterback, J. K.; Ruzicka, J. L.; Keller, H. R.; Pellows, L. M.; Dukovic, G. Electron Transfer from Semiconductor Nanocrystals to Redox Enzymes. *Annu. Rev. Phys. Chem.* **2020**, *71* (1), 335−359.
(16) Ding, T. X.; Olshansky, J. H.; Leone, S. R.; Alivisatos, A. P. Efficiency of Hole Transfer from Photoexcited Quantum Dots to Covalently Linked Molecular Species. *J. Am. Chem. Soc.* **2015**, *137* (5), 2021−2029.
(17) Morris-Cohen, A. J.; Frederick, M. T.; Cass, L. C.; Weiss, E. A. Simultaneous Determination of the Adsorption Constant and the Photoinduced Electron Transfer Rate for a Cds Quantum Dot−Viologen Complex. *J. Am. Chem. Soc.* **2011**, *133* (26), 10146−10154.
(18) Sykora, M.; Petruska, M. A.; Alstrum-Acevedo, J.; Bezel, I.; Meyer, T. J.; Klimov, V. I. Photoinduced Charge Transfer between CdSe Nanocrystal Quantum Dots and Ru−Polypyridine Complexes. *J. Am. Chem. Soc.* **2006**, *128* (31), 9984−9985.
(19) Huang, J.; Stockwell, D.; Huang, Z.; Mohler, D. L.; Lian, T. Photoinduced Ultrafast Electron Transfer from CdSe Quantum Dots to Re-Bipyridyl Complexes. *J. Am. Chem. Soc.* **2008**, *130* (17), 5632−5633.
(20) Robel, I.; Subramanian, V.; Kuno, M.; Kamat, P. V. Quantum Dot Solar Cells. Harvesting Light Energy with CdSe Nanocrystals Molecularly Linked to Mesoscopic TiO_2 Films. *J. Am. Chem. Soc.* **2006**, *128* (7), 2385−2393.
(21) Hines, D. A.; Forrest, R. P.; Corcelli, S. A.; Kamat, P. V. Predicting the Rate Constant of Electron Tunneling Reactions at the CdSe−TiO_2 Interface. *J. Phys. Chem. B* **2015**, *119* (24), 7439−7446.
(22) Xu, Z.; Cotlet, M. Quantum Dot-Bridge-Fullerene Heterodimers with Controlled Photoinduced Electron Transfer. *Angew. Chem., Int. Ed.* **2011**, *50* (27), 6079−6083.
(23) Wang, H.; McNellis, E. R.; Kinge, S.; Bonn, M.; Cánovas, E. Tuning Electron Transfer Rates through Molecular Bridges in Quantum Dot Sensitized Oxides. *Nano Lett.* **2013**, *13* (11), 5311−5315.
(24) Zhu, H.; Yang, Y.; Wu, K.; Lian, T. Charge Transfer Dynamics from Photoexcited Semiconductor Quantum Dots. *Annu. Rev. Phys. Chem.* **2016**, *67* (1), 259−281.
(25) Zhou, Y.; Fuentes-Hernandez, C.; Shim, J.; Meyer, J.; Giordano, A. J.; Li, H.; Winget, P.; Papadopoulos, T.; Cheun, H.; Kim, J.; Fenoll, M.; Dindar, A.; Haske, W.; Najafabadi, E.; Khan, T. M.; Sojoudi, H.; Barlow, S.; Graham, S.; Brédas, J.-L.; Marder, S. R.; Kahn, A.; Kippelen, B. A Universal Method to Produce Low−Work Function Electrodes for Organic Electronics. *Science* **2012**, *336* (6079), 327−332.
(26) Paniagua, S. A.; Giordano, A. J.; Smith, O. L.; Barlow, S.; Li, H.; Armstrong, N. R.; Pemberton, J. E.; Brédas, J.-L.; Ginger, D.; Marder, S. R. Phosphonic Acids for Interfacial Engineering of Transparent Conductive Oxides. *Chem. Rev.* **2016**, *116* (12), 7117−7158.
(27) Hotchkiss, P. J.; Jones, S. C.; Paniagua, S. A.; Sharma, A.; Kippelen, B.; Armstrong, N. R.; Marder, S. R. The Modification of Indium Tin Oxide with Phosphonic Acids: Mechanism of Binding, Tuning of Surface Properties, and Potential for Use in Organic Electronic Applications. *Acc. Chem. Res.* **2012**, *45* (3), 337−346.
(28) Kim, D.; Lee, A. W. H.; Eastcott, J. I.; Gates, B. D. Modifying the Surface Properties of Indium Tin Oxide with Alcohol-Based Monolayers for Use in Organic Electronics. *ACS Appl. Nano Mater.* **2018**, *1* (5), 2237−2248.
(29) Boucher, D. G.; Kearney, K.; Ertekin, E.; Rose, M. J. Tuning *p*-Si(111) Photovoltage via Molecule|Semiconductor Electronic Coupling. *J. Am. Chem. Soc.* **2021**, *143* (6), 2567−2580.
(30) Seo, J.; Kim, H. J.; Pekarek, R. T.; Rose, M. J. Hybrid Organic/Inorganic Band-Edge Modulation of *p*-Si(111) Photoelectrodes: Effects of R, Metal Oxide, and Pt on H_2 Generation. *J. Am. Chem. Soc.* **2015**, *137* (9), 3173−3176.
(31) Brown, P. R.; Kim, D.; Lunt, R. R.; Zhao, N.; Bawendi, M. G.; Grossman, J. C.; Bulović, V. Energy Level Modification in Lead Sulfide Quantum Dot Thin Films through Ligand Exchange. *ACS Nano* **2014**, *8* (6), 5863−5872.
(32) Kroupa, D. M.; Vörös, M.; Brawand, N. P.; McNichols, B. W.; Miller, E. M.; Gu, J.; Nozik, A. J.; Sellinger, A.; Galli, G.; Beard, M. C. Tuning Colloidal Quantum Dot Band Edge Positions through Solution-Phase Surface Chemistry Modification. *Nat. Commun.* **2017**, *8* (1), 15257.
(33) Wu, X.; Xie, S.; Liu, C.; Zhou, C.; Lin, J.; Kang, J.; Zhang, Q.; Wang, Z.; Wang, Y. Ligand-Controlled Photocatalysis of CdS Quantum Dots for Lignin Valorization under Visible Light. *ACS Catal.* **2019**, *9* (9), 8443−8451.
(34) Tagliazucchi, M.; Tice, D. B.; Sweeney, C. M.; Morris-Cohen, A. J.; Weiss, E. A. Ligand-Controlled Rates of Photoinduced Electron Transfer in Hybrid CdSe Nanocrystal/Poly(Viologen) Films. *ACS Nano* **2011**, *5* (12), 9907−9917.
(35) Weinberg, D. J.; He, C.; Weiss, E. A. Control of the Redox Activity of Quantum Dots through Introduction of Fluoroalkanethiolates into Their Ligand Shells. *J. Am. Chem. Soc.* **2016**, *138* (7), 2319−2326.
(36) De Roo, J.; Yazdani, N.; Drijvers, E.; Lauria, A.; Maes, J.; Owen, J. S.; Van Driessche, I.; Niederberger, M.; Wood, V.; Martins, J. C.; Infante, I.; Hens, Z. Probing Solvent−Ligand Interactions in Colloidal Nanocrystals by the NMR Line Broadening. *Chem. Mater.* **2018**, *30* (15), 5485−5492.
(37) Jones, B. A.; Facchetti, A.; Wasielewski, M. R.; Marks, T. J. Tuning Orbital Energetics in Arylene Diimide Semiconductors. Materials Design for Ambient Stability of n-Type Charge Transport. *J. Am. Chem. Soc.* **2007**, *129* (49), 15259−15278.
(38) Djurovich, P. I.; Mayo, E. I.; Forrest, S. R.; Thompson, M. E. Measurement of the Lowest Unoccupied Molecular Orbital Energies of Molecular Organic Semiconductors. *Org. Electron.* **2009**, *10* (3), 515−520.

https://doi.org/10.1021/acs.jpclett.1c03825
J. Phys. Chem. Lett. 2022, 13, 1416−1423

(39) Jasieniak, J.; Califano, M.; Watkins, S. E. Size-Dependent Valence and Conduction Band-Edge Energies of Semiconductor Nanocrystals. *ACS Nano* **2011**, *5* (7), 5888−5902.
(40) Kroupa, D. M.; Vörös, M.; Brawand, N. P.; Bronstein, N.; McNichols, B. W.; Castaneda, C. V.; Nozik, A. J.; Sellinger, A.; Galli, G.; Beard, M. C. Optical Absorbance Enhancement in PbS QD/Cinnamate Ligand Complexes. *J. Phys. Chem. Lett.* **2018**, *9* (12), 3425−3433.
(41) Marcus, R. A. On the Theory of Oxidation-Reduction Reactions Involving Electron Transfer. I. *J. Chem. Phys.* **1956**, *24* (5), 966−978.
(42) Zhu, H.; Yang, Y.; Hyeon-Deuk, K.; Califano, M.; Song, N.; Wang, Y.; Zhang, W.; Prezhdo, O. V.; Lian, T. Auger-Assisted Electron Transfer from Photoexcited Semiconductor Quantum Dots. *Nano Lett.* **2014**, *14* (3), 1263−1269.
(43) Klimov, V. I. Spectral and Dynamical Properties of Multiexcitons in Semiconductor Nanocrystals. *Annu. Rev. Phys. Chem.* **2007**, *58*, 635−673.
(44) Yang, Y.; Rodríguez-Córdoba, W.; Lian, T. Ultrafast Charge Separation and Recombination Dynamics in Lead Sulfide Quantum Dot−Methylene Blue Complexes Probed by Electron and Hole Intraband Transitions. *J. Am. Chem. Soc.* **2011**, *133* (24), 9246−9249.
(45) Cho, B.; Peters, W. K.; Hill, R. J.; Courtney, T. L.; Jonas, D. M. Bulklike Hot Carrier Dynamics in Lead Sulfide Quantum Dots. *Nano Lett.* **2010**, *10* (7), 2498−2505.
(46) Bender, J. A.; Raulerson, E. K.; Li, X.; Goldzak, T.; Xia, P.; Van Voorhis, T.; Tang, M. L.; Roberts, S. T. Surface States Mediate Triplet Energy Transfer in Nanocrystal−Acene Composite Systems. *J. Am. Chem. Soc.* **2018**, *140* (24), 7543−7553.
(47) Ford, W. E.; Hiratsuka, H.; Kamat, P. V. Photochemistry of 3, 4, 9, 10-Perylenetetracarboxylic Dianhydride Dyes. 4. Spectroscopic and Redox Properties of Oxidized and Reduced Forms of the Bis(2, 5-Di-Tert-Butylphenyl)Imide Derivative. *J. Phys. Chem.* **1989**, *93* (18), 6692−6696.
(48) Gosztola, D.; Niemczyk, M. P.; Svec, W.; Lukas, A. S.; Wasielewski, M. R. Excited Doublet States of Electrochemically Generated Aromatic Imide and Diimide Radical Anions. *J. Phys. Chem. A* **2000**, *104* (28), 6545−6551.
(49) Marcon, R. O.; Brochsztain, S. Aggregation of 3,4,9,10-Perylenediimide Radical Anions and Dianions Generated by Reduction with Dithionite in Aqueous Solutions. *J. Phys. Chem. A* **2009**, *113* (9), 1747−1752.
(50) Hedström, S.; Chaudhuri, S.; La Porte, N. T.; Rudshteyn, B.; Martinez, J. F.; Wasielewski, M. R.; Batista, V. S. Thousandfold Enhancement of Photoreduction Lifetime in Re(bpy)$(CO)_3$ via Spin-Dependent Electron Transfer from a Perylenediimide Radical Anion Donor. *J. Am. Chem. Soc.* **2017**, *139* (46), 16466−16469.
(51) Kaledin, A. L.; Lian, T.; Hill, C. L.; Musaev, D. G. A Hybrid Quantum Mechanical Approach: Intimate Details of Electron Transfer between Type-I CdSe/ZnS Quantum Dots and an Anthraquinone Molecule. *J. Phys. Chem. B* **2015**, *119* (24), 7651−7658.
(52) Morris-Cohen, A. J.; Aruda, K. O.; Rasmussen, A. M.; Canzi, G.; Seideman, T.; Kubiak, C. P.; Weiss, E. A. Controlling the Rate of Electron Transfer between a Quantum Dot and a Tri-Ruthenium Molecular Cluster by Tuning the Chemistry of the Interface. *Phys. Chem. Chem. Phys.* **2012**, *14* (40), 13794.
(53) Hyun, B.-R.; Bartnik, A. C.; Lee, J.-K.; Imoto, H.; Sun, L.; Choi, J. J.; Chujo, Y.; Hanrath, T.; Ober, C. K.; Wise, F. W. Role of Solvent Dielectric Properties on Charge Transfer from PbS Nanocrystals to Molecules. *Nano Lett.* **2010**, *10* (1), 318−323.
(54) Lian, S.; Weinberg, D. J.; Harris, R. D.; Kodaimati, M. S.; Weiss, E. A. Subpicosecond Photoinduced Hole Transfer from a CdS Quantum Dot to a Molecular Acceptor Bound Through an Exciton-Delocalizing Ligand. *ACS Nano* **2016**, *10* (6), 6372−6382.
(55) Morris-Cohen, A. J.; Peterson, M. D.; Frederick, M. T.; Kamm, J. M.; Weiss, E. A. Evidence for a Through-Space Pathway for Electron Transfer from Quantum Dots to Carboxylate-Functionalized Viologens. *J. Phys. Chem. Lett.* **2012**, *3* (19), 2840−2844.
(56) Green, P. B.; Yarur Villanueva, F.; Imperiale, C. J.; Hasham, M.; Demmans, K. Z.; Burns, D. C.; Wilson, M. W. B. Directed Ligand Exchange on the Surface of PbS Nanocrystals: Implications for Incoherent Photon Conversion. *ACS Appl. Nano Mater.* **2021**, *4* (6), 5655−5664.

https://doi.org/10.1021/acs.jpclett.1c03825
J. Phys. Chem. Lett. 2022, 13, 1416−1423